Silicon (2020) 12:373–380
https://doi.org/10.1007/s12633-019-00140-6

ORIGINAL PAPER

Optical and Optoelectronic Properties Enhancement of Porous Silicon Treated with Indium Oxide

Fakher Laatar[1,2] · Afef Harizi[2,3] · Hatem Ezzaouia[1]

Received: 23 December 2018 / Accepted: 18 March 2019 / Published online: 26 March 2019

Abstract

This paper presents the results of the effect of Indium oxide (In_2O_3) on the structural, optical, and optoelectronic properties of porous silicon (PS). The results show an important improvement of optoelectronic property of PS coated with In_2O_3 as a antireflective thin film. The treated PS with In_2O_3 thin film was thermally annealed at various temperatures to improve the efficiency of the photovoltaic cells. The deposition of In_2O_3 onto the PS sample was performed by simple immersion method. Surface morphology and chemical composition modification of the samples In_2O_3/PS were analyzed by SEM, EDX, and FTIR spectroscopy. Total reflectivity of In_2O_3/PS layers decreases significantly compared to as-prepared PS owing to an improvement in the light absorption. The PS treated with In_2O_3 shows a significant enhancement in the minority carrier lifetime (τ_{eff}) indicating an improved surface quality in comparison with the untreated PS. Photoluminescence (PL) measurements of PS layer treated with In_2O_3 has revealed an increase in PL-intensity and a bleu shift in emission PL band as a function of annealing temperature. The PL and τ_{eff} enhancement are due to the surface passivation improvement and the decrease of recombination process.

Keywords Porous silicon · Indium oxide · Reflectivity · Photoluminescence · Lifetime

Highlights
- In_2O_3 coated PS decreases the reflectivity significantly from 30 % to 2.4 %.
- The effective minority carrier lifetime increases from 1.85 μs to 16.4 μs after treatment of PS with In_2O_3.
- FTIR analysis showed a substitution of Si-H bonds to Si-O-Si and Si-O-In after the thermal annealing.
- Annealing temperature of In_2O_3/PS composite at 300 °C leads to a noticeable improvement in PL intensity.
- A blueshift was obtained in the PL spectra due to the increase in the concentration of oxygen atoms and the quantum confinement effect of the oxidized silicon nanocrystals after thermal oxidation.

✉ Fakher Laatar
fakher8laatar@gmail.com

[1] Laboratory of Semiconductors, Nanostructures and Advanced Technology, Center for Research and Technology Energy, Tourist Route Soliman, BP 95, 2050 Hammam-Lif, Tunisia

[2] Department of Physics, Faculty of Education of Afif, Shaqra University, Shaqra, Saudi Arabia

[3] Laboratoire de Photovoltaïque et Matériaux Semiconducteurs, ENIT-Université Tunis ElManar, BP 37, Le belvédère, 1002 Tunis, Tunisie

1 Introduction

Porous silicon (PS) thin film has received considerable attention due to its large range of applications such as solar cells [1], opto-electronic [2–5], chemical and biological sensors [6–11], and biomedical devices [12]. However, the surface of PS layer can be oxidized in natural atmosphere which may change their chemical structure and optical properties [13, 14]. To remedy this problem, many authors have indicated that the deposition of conducting material such as Cu, Ni, Au, Fe, Ag, Li, and Zn [15–22] in the pores of PS layer enhance their photoluminescence and electrical properties. These different metals were deposited on PS layers by using various methods including thermal evaporation, sputtering, electrochemical, electrolyses and immersing plating. Various chemical and physical methods have been used to fabricate In_2O_3 thin films, such as laser deposition [16], atomic layer deposition [17], electrochemical deposition [18], sputtering [19], and chemical vapor deposition [20]. These different deposition methods have been widely used for thin film preparation due to accurate control of deposition parameters [21, 23–25]. Howeover, only specified thin film area can be obtained due to

the limitation of equipements of each deposition technique [14–21]. In contrast, thin film deposition via chemical routes such as chemical bath, spin-coating and immersing methods are competitive alternatives to the conventional physical deposition techniques. It has been reported that the immersing of PS layer is a suitable method for large-area deposition of thin films, due to it is low-cost and the fact that it is very easy and more practical in comparison with other methods [15–18, 23, 24].

Indium oxide (In_2O_3) is an attractive semiconducting material due to its wide band-gap (3.7 eV) and their high transmittance in the visible range (>90%) [25], which are used for many applications in nano-devices, such as solar cells [26], optoelectronic [27], and gas sensors [28, 29].

Several investigations of the origin and mechanism of light emission of In_2O_3 thin film in glass and silicon substrates have been carried out by PL studies. But, the influences of this film on the photoluminescence and optoelectronic properties of PS layer have not been studied yet.

This paper examine the passivation of PS by immersion in indium solution and the thermal annealing effect on the physical properties of PS layer treated with In_2O_3, specially the reflectivity, the photoluminescence and the minority carrier lifetime.

2 Experimental Details

The study has been carried out on *p*-type boron doped monocrystalline silicon substrates with a cristallographic orientation of (100) and a resistivity of 1–2 Ω.cm. PS layers were fabricated by a two-step anodizing process using electrochemical anodization in a solution of HF(20%)/C_2H_5OH (1:1) under stirring at a constant current density of 5 mA/cm^2 for an etching time of 3 min. The initial PS formed on the silicon substrate was removed by chemical etching using a NaOH solution and followed by rinsing in bi-distilled water and drying under N_2. The second electrochemical anodization step was performed in a solution of HF(40%)/C_2H_5OH (1:1) under stirring at a current density of 15 mA/cm^2 during 7 min in order to obtain a PS layer with a homogeneous pores structure. The formed PS layers were cleaned in a double deionized water in order to remove the residual acid and dried under N_2. In a typical experiment, two drops of 0.02 M indium (III) chloride butahydrate ($InCl_3{\cdot}4H_2O$ dissolved in 0.12 M hydrochloric acid solution) aqueous solution were added onto a PS layer at room temperature. The In_2O_3/PS multilayers were obtained by depositing solution dropwise onto PS substrates under 2500 rpm for 1 min by a spin coater and then dried at a heater plate at 100 °C for 10 min to evaporate the solvents. Finally, the samples were annealed at 200, 300, and 500 °C in an infrared furnace under air atmosphere for 90 min.

Scanning Electron Microscope (ZEISS Ultra Plus) was used to study the structures of PS layer before and after treatment with indium oxide. EDX analysis was performed to identify the elements composition of PS and In_2O_3/PS layers. The composition of PS and In_2O_3/PS samples was analyzed by Fourier transfer infrared (FTIR) spectroscopy in the 2200~400 cm^{-1} spectral range using a 560 Nicolet-Magna spectrometer. The optical reflectivity spectra of samples was examined in the wavelength range 300–1200 nm using a UV/VIS/NIR Perkin-Elmer (Lambda 950) spectrophotometer. Photoluminescence measurements were carried out at room temperature and were registered on a PL (LS 55) Perkin-Elmer spectrometer using a Xe light source with a λ_{exc} of 447 nm. Furthermore, the effective minority carrier lifetime was identified using the photoconductivity method by a Sinton WTC-120 set-up.

3 Results and Discussions

3.1 SEM and EDX Analyses

Figure 1a shows the SEM image of untreated PS sample. From this image, we observe a nonuniform distribution of

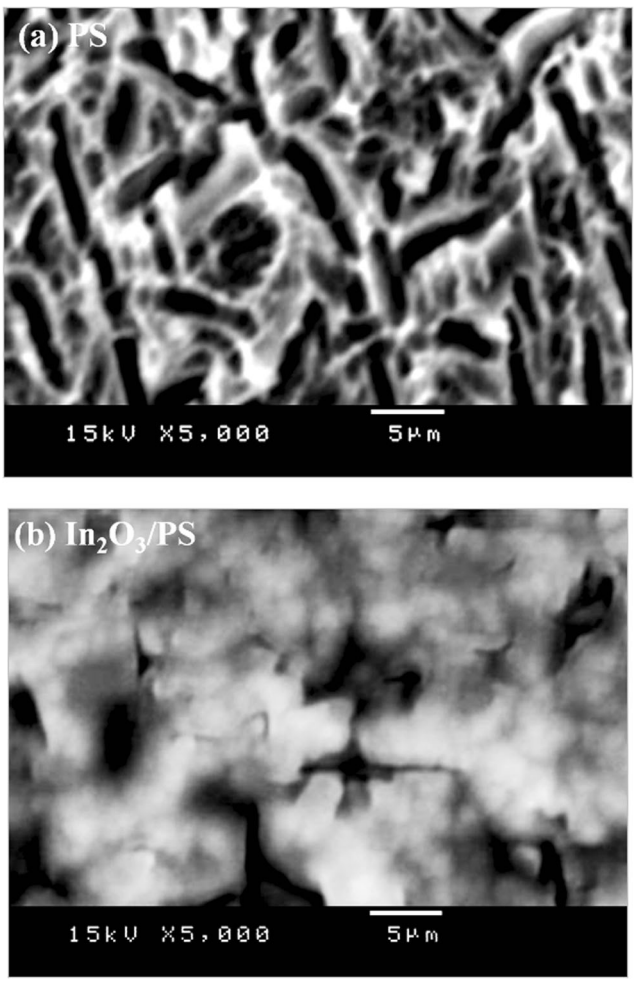

Fig. 1 SEM images of top view of a PS layer and annealed In_2O_3/PS sample at 200 °C

micropores with a ravines form on the surface of PS layer. Figure 1b shows SEM image of the treated PS layer with In_2O_3. This figure exhibits a homogeneous distribution of In_2O_3 clusters with some voids percentage that covered all the surface of PS layer.

In this study, EDX analysis was performed to report the elements composition presented in the samples of PS layer and In_2O_3/PS (see Table 1). Figure 2a and b exhibit the EDX pattern of PS and In_2O_3/PS layers, and the relative elements composition of the samples were depicted in Table 1 below their corresponding spectra. In Fig. 2a, the spectrum of PS sample presents the O and Si elements, which confirms that the layer is made of silicon oxide forming the PS. In Fig. 2b, EDX spectrum of In_2O_3/PS sample shows the expected elements: Si, In, and O. However, the PS surface treated with indium oxide mainly consisted of Si presented by a high intensity peak centered at 1.88 keV. The characteristic peaks of In and O elements are present in the treated sample, which are attributed to indium oxide deposition on PS.

3.2 FTIR Spectroscopic Analysis

In this work, FTIR spectroscopy was ridiculed to reveal the chemical bond structure of In_2O_3/PS composites. Figure 3 shows the FTIR spectra of PS, as-deposited and annealed samples of In_2O_3/PS at different temperature (from 200 to 500 °C). The vibration bonds at about 1080 cm^{-1} and 1182 cm^{-1} correspond to stretch modes of Si–O–Si and Si–O, respectively. The large vibration band in the range 610–660 cm^{-1} is a mixture of stretching mode Si–Si and wagging mode Si–H_n ($n = 1; 2$). The vibration bonds centered at 842 cm^{-1} and 977 cm^{-1} are attributed to scissors mode Si–H_2 and wagging mode O_3Si–H, respectively. All the peaks obtained in Fig. 3 are in compliance with the previous data mentioned in the literature [30–35]. Important changes in the FTIR spectrum after deposition of In_2O_3 on PS can be seen in comparison with the untreated porous layer. These changes are pronounced particularly in Si–H and Si–O absorption peaks. We observe an increase in the peak intensity of the stretching mode Si–O–Si located at 1182 cm^{-1}. Moreover, the peaks intensity of Si–H_x ($x = 1; 2$) at 2083 and 2114 cm^{-1} decrease in the case of as-deposited In_2O_3 on PS layer. After annealing In_2O_3/PS, the intensity of Si–O bonds related asymmetric stretching modes and located in the range 1000–1300 cm^{-1} increase significantly, while the peaks intensity of Si–H_x located at

Table 1 Elemental composition of PS and In_2O_3/PS layers

Sample element	PS		In_2O_3/PS		
	O K	Si K	O K	In L	Si K
Weight %	22.72	77.28	23.13	20.23	56.64
Atomic %	28.18	71.82	39.35	8.24	52.41

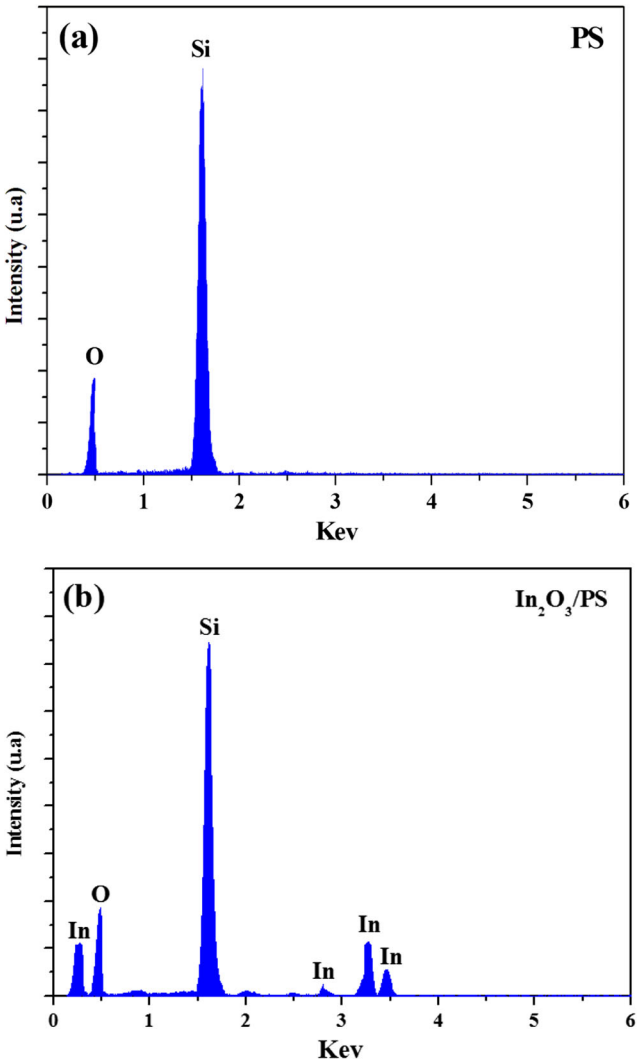

Fig. 2 Typical EDX spectra of PS and In_2O_3/PS layers

2083 cm^{-1} and 2114 cm^{-1} have decreased progressively as a function of annealing temperature. The increase in the intensity and width of the absorption peak related Si–O–Si and the decrease of the peaks of Si–H_n are presumably caused by the hydrogen atoms replacement with oxygen and/or Indium atoms. As reported in the literature, the metal–oxygen–silicon bonding is located in the wavenumber range 300–700 cm^{-1} [36, 37].

The new vibration mode that appeared at 784 cm^{-1} after deposition of In_2O_3 on PS, corresponds to the O-Si-O bending mode [38]. The vibration mode observed at 598 cm^{-1} after annealing can be attributed to the formation of In–O bond [39].

After the deposition and annealing temperature of In_2O_3/PS, the FTIR spectra shows the appearance of new peak centered at 460 cm^{-1}, which can be the result of interaction between the In_2O_3 and PS interfaces. Therefore, the peak centered at 460 cm^{-1} can be assigned to In-O-Si bonding. FTIR analysis indicates that Si–O bonds take place instead of the unstable Si–H bonds after deposition of In_2O_3 onto the PS

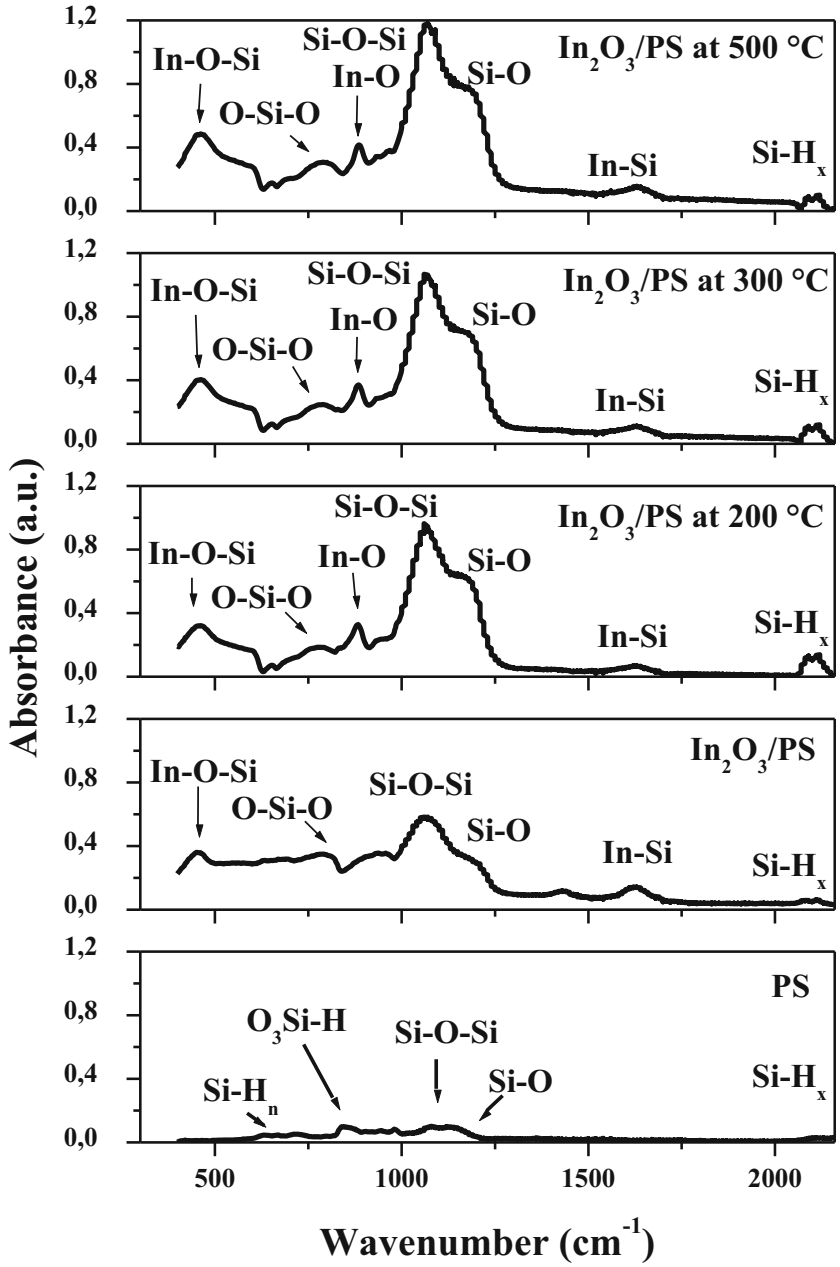

Fig. 3 FTIR spectra of the treated PS layer with indium oxide at different temperature

layer resulting in a surface oxidation. Thermal treatment of In_2O_3/PS composite at high temperatures under air also enhances the surface. Therefore, the increase in the absorption peaks intensity of Si-O-Si and In-O-Si can be attributed to the increase in the concentration of oxygen atoms into the In_2O_3/PS composite as a function of annealing temperature.

3.3 Total Reflectivity Analysis

The reflectivity spectra of untreated PS, as-prepared and annealed In_2O_3/PS at various temperature (200 °C, 300 °C, and 500 °C), are saved in the wavelength region 300–1200 nm, as shown in Fig. 4. As well-known, the reflected optical field with multiple passes is principally related to the contribution of front and backside surfaces through the antireflective film. Several published works focused on the study of different nanostructured materials, such as metals and metals oxide as antireflective structures for the efficiency enhancement of photovoltaic cells. For instance, Bouzoura et al, F. Habubi et al., and Ahmadivand et al. have obtained the following result: the SnO_2, Zn_3P_2, and Ag with an ultrathin structures provide an average reflectance of 24%, 25.35%, and 26%, repectively, for a wavelength range of 300–1200 nm [40–42]. In an analogous condition, the metal oxide In_2O_3 nanocrystals as a antireflective coating yield ~22.6% of average reflectance for a similar wavelength range. On the basis of these

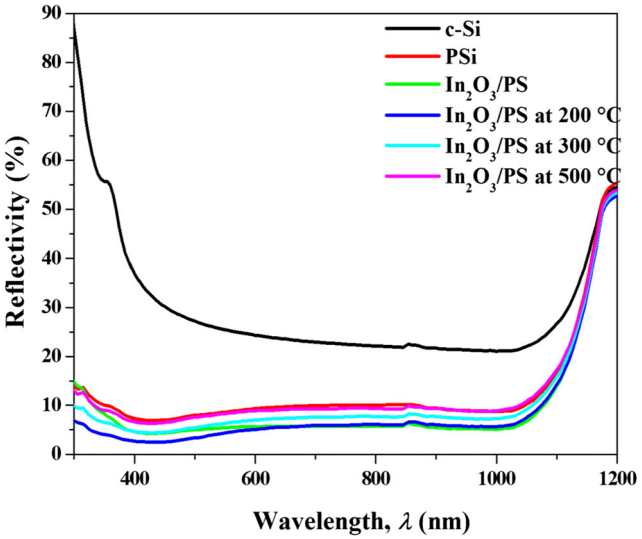

Fig. 4 Reflectivity spectra of PS, as-deposited In_2O_3 on PS, and annealed In_2O_3/PS at different temperatures (200, 300 and 500 °C)

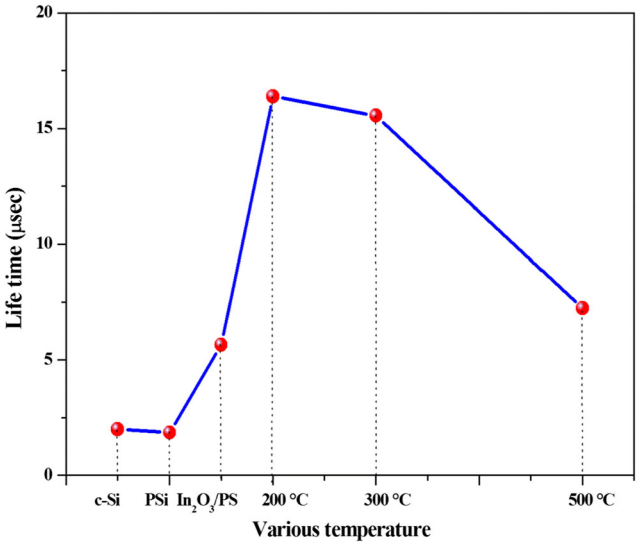

Fig. 5 Minority carrier lifetime measurement after each process: untreated PS, and In_2O_3/PS before and after heat treatment

investigations, we note that the metals oxide films provide a high reflectance percentage compared to the metals or metals-alloys. So, in the beggining we examine the absorption efficiency of Indium oxide film in c-Si and then, we study the annealing effect on the c-Si/In_2O_3 nanocrystals to yield an efficient antireflective nanostructure. Annealing temperature has a significant effect on the surface morpholgy and optical property of the In_2O_3/PS films. Therefore, the annealing process activates the diffusion of In_2O_3 inside the PS layer [43–45], which may lead to enhancing the surface passivation quality of the PS.

The porosity of the PS layer reduces the reflection loss, allowing the light trapping within the cell by internal multi-reflection. Furthermore, the treated PS layer with Indium oxide shows a significant reflection loss in the visible wavelength range. The sample annealed at 200 °C exhibits the most excellent reduction of surface reflectivity from 30 to 2.4% in the visible light range 400–800 nm. The significant reduction in the reflectivity of annealed In_2O_3/PS compared to the untreated PS and other samples annealed at 300 and 500 °C may be the result of textured surface enhancement. Therefore, this antireflection coating can be used as a light trapping to improve the efficiency of the photovoltaic cells.

3.4 Minority-Carrier Lifetime Measurements

To study the influence of In_2O_3/PS on the electronic quality of the silicon substrate, we measured the effective carrier lifetime (τ_{eff}), before and after heat treatment. Figure 5 shows the enhancement of the τ_{eff} as a function of the annealed In_2O_3/PS samples. For PS sample, the obtained results indicate a slight decrease of the τ_{eff} compared to that for the c-Si substrate due to the increase of defects onto the porous layer. The treated PS with In_2O_3 shows an improvement in the effective lifetime from 1.85 μs (for PSi) to 16.4 μs (for annealed In_2O_3/PS at 200 °C). The further increase in annealing temperature causes the degradation of effective minority carrier lifetime to 7.2 μs at 500 °C. The improvement in the effective lifetime could be attributed to surface passivation and the minimization of the dangling bonds density at the c–Si surface. This enhancement is mainly due to the coordination of In atoms to the Si atoms through the oxygen (In–O–Si bonds) as indicated in the FTIR analysis.

3.5 PL Spectroscopic Analysis

The Photoluminescence (PL) measurements of PS and In_2O_3/PS layers were carried out at a room temperature with 447 nm wavelength from a Xe lamp source. PL spectra of PS layer, as-deposited and annealed In_2O_3/PS samples at various temperatures (from 200 to 500 °C) as a function of photon energy are showed in Fig. 6. As shown in this figure, the untreated PS sample exhibits a PL band centered at 1.86 eV. The PL spectra of as-prepared and annealed In_2O_3/PS samples exhibit orange-red emission bands centerted between 1.98 eV (626 nm) and 1.88 eV (659 nm). The origin of this orange-red emission is attributed to the quantum confinement of silicon oxide nanocrystals forming the PS layer and the interface state between indium oxide and the silicon oxide films, as shown in the FTIR analysis. In Fig. 6, the PL result shows a significant improvement after depositing In_2O_3 onto PS and annealing In_2O_3/PS at 200 °C and 300 °C compared to PS sample. This reveals an increase in PL-band intensity and a bleu shift from 1.88 eV (for as-prepared In_2O_3/PS) to 1.98 eV (for annealed In_2O_3/PS at 500 °C). The origin of these changes can be attributed

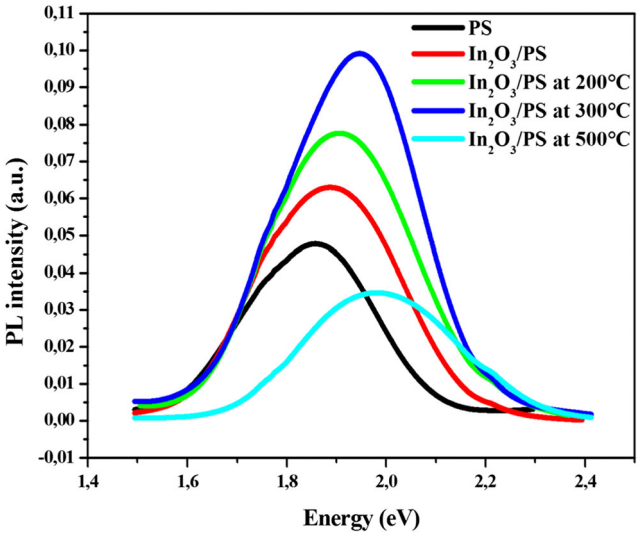

Fig. 6 PL spectra of PS, as-deposited and annealed In_2O_3/PS at 200, 300, and 500 °C

to the increase in the concentration of oxygen atoms incorporated into In_2O_3/PS and the quantum confinement effect of the oxidized silicon nanocrystals. The enhancement of the PL spectra of In_2O_3/PS structure is due to the surface passivation improvement and the decrease of recombination activities. Afterward, the PL intensity decreases significantly after sample annealing at 500 °C, due to the outflowing of impurities up to the surface of Si nanocrystals. The large decrease of the PL intensity at this annealing temperature can be related to defect states at Si and Si oxide interface, resulting the diffusin of impurities and the formation of nonradiative recombination sites. These higher temperatures promote the decrease in the void concentration of assembly In_2O_3/PS, leading to the obtaining of a compact microstructure [46]. The shift to higher energy can also be attribute to the trapped electrons at the located states owing to Si = O bond of PS layer [47–49] and the substitution of hydrogen atoms by the oxygen atoms [49, 50] and/or the oxidized indium forming In-O-Si according to the FTIR analysis.

From the above PL and FTIR discussions, we may deduce that the enhancement in the peaks intensity is related to an increase in the number of Si–metals (In) bonds. It is shown that annealing temperature at 200 °C and 300 °C has a significant influence on the peaks intensity of PL and FTIR, which is in good agreement with the carrier lifetime (τ_{eff}) and indicates the presence of a passivation process of the PS structure. Table 2 presents a comparative data of FTIR, Reflectivity, PL, minority carrier lifetime, and conversion efficiency characteristics of PS treated with different materials [22, 43, 44, 51, 52]. This table shows similar physical characteristics for different materials used for Si solar cells improvement. Furtermore, from the values of conversion efficiency of these materials, we can conclude that the efficiency of the photvoltaic cell (PS treated with the Indium oxide) does not exceed 10%. Therefore, the In_2O_3 films can be used as a suitable antireflection and passivation coating for c-Si solar cells.

4 Conclusion

This paper have exposed the influence of thermal annealing on the optical and optoelectronic properties of In_2O_3/PS layers. In_2O_3/PS samples thermally annealed at 200 °C present a low average reflectance of 2.4%. FTIR spectroscopy measurements have shown the increase of Si–O–Si and Si-O-In bonds intensity with the increase of annealing temperature of In_2O_3/PS film, and found to be a replacement of Si-H bonds. A modification in the surface morphology of PS layer after treatment with In_2O_3 is observed. Annealing temperature of In_2O_3/PS composite at 200 °C leads to a noticeable improvement in carrier lifetime (from 1.85 μs to 16.4 μs). The paper has also demonstrated that the treatment of PS with In_2O_3 causes an improvement in PL intensity. The treatment of PS layer with In_2O_3 acts as an efficient antireflection coating. The thermal annealing of In_2O_3/PS sample leads to dangling bonds passivation at the surface of PS layer.

Table 2 Physical parameters of PS treated with different materials as a antireflective coating

Material	Reflectivity R (%)	Peak intensity of Si-O-Metal (a.u.)	Photoluminescence peak intensity (a.u.)	Minority carrier lifetime τ_{eff} (μs)	Conversion efficiency η (%)
In_2O_3 [This work]	2.4	0.4	0.099	16.4	–
V_2O_5 [43]	5	1.1	0.026	134.74	12.5
LiBr [44]	7	0.05	0.03	18.2	–
ZnO [22]	4	–	–	–	20
NiO [51]	5	0.7	0.04	–	–
Er_2O_3 [52]	7	0.4	0.17	56	7.9
Al_2O_3 [53]	9	–	–	90	12

Acknowledgements This work was funded by the Ministry of Higher Education and Scientific Research of Tunisia.

References

1. Hang BR, Yang YK, Lin TC, Yang WL (2012) A simple and low-cost technique for silicon nanowire arrays based solar cells. Sol Energy Mater Sol Cells 98:357–362
2. Ahmadi MT, Lau HH, Ismail R, Arora VK (2009) Current–voltage characteristics of a silicon nanowire transistor. Microelectron J 40: 547–549
3. Collins RT, Fauchet PM, Tischler MA (1997) Porous silicon: from luminescence to LEDs. Phys Today 50:24–31
4. Lazarouk S, Jaguiro P, Katsouba S (1996) Stable electroluminescence from reverse biased *n*-type porous silicon–aluminum Schottky junction device. Appl Phys Lett 68:2108–2110
5. Steiner P, Kozlowski F, Lang W (1993) Light-emitting porous silicon diode with an increased electroluminescence quantum efficiency. Appl Phys Lett 62:2700–2702
6. Zhang GJ, Ning Y (2012) Silicon nanowire biosensor and its applications in disease diagnostics: a review. Anal Chim Acta 749:1–15
7. Foucaran A, Pascal-Delannoy F, Giani A, Sackda A, Combette P, Boyer A (1997) Porous silicon layers used for gas sensor applications. Thin Solid Films 297:317–320
8. Sailor MJ, Link JR (2005) "Smart dust": nanostructured devices in a grain of sand. Chem Commun 94:1375
9. Chan S, Fauchet PM, Li Y, Rothberg LJ, Miller BL (2000) Porous silicon microcavities for biosensing applications. Phys Status Solidi A 182:541–546
10. Lin VSY, Motesharei K, Dancil KS, Sailor MJ, Ghadiri MR (1997) A porous silicon-based optical interferometric biosensor. Science 278:840–843
11. Thust M, Schoning MJ, Frohnhoff S, Arens-Fischer R (1996) Porous silicon as a substrate material for potentiometric biosensors. Meas Sci Technol 7:26–29
12. Coffer JL, Whitehead MA, Nagesha DK, Mukherjee P, Akkaraju G, Totolici M, Saffie RS, Canham LT (2005) Porous silicon-based scaffolds for tissue engineering and other biomedical applications. Phys Status Solidi A 202:1451–1455
13. Kim HS, Kim MG, Ha YG, Kanatzidis MG, Marks TJ, Facchetti A (2009) Low-temperature solution-processed amorphous indium tin oxide field-effect transistors. J Am Chem Soc 131:10826–10827
14. Park JS, Song JI, Heo YW, Lee JH, Kim JJ, Lim WT, Stafford L, Norton DP, Pearton SJ (2006) Effects of Zn content on structural and transparent conducting properties of indium–zinc oxide films grown by rf magnetron sputtering. J Vac Sci Technol B 24:2737–2740
15. Im J, Auciello O, Baumann PK, Streiffer SK, Kaufman DY, Krauss AR (2000) Composition-control of magnetron-sputter-deposited $(Ba_xSr_{1-x})Ti_{1+y}O_{3+z}$ thin films for voltage tunable devices. Appl Phys Lett 76:625–627
16. Wang CH, Cimalla V, Romanus H, Kups T, Niebelchutz M, Ambacher O (2007) Tuning of electrical and structural properties of indium oxide films grown by metal organic chemical vapor deposition. Thin Solid Films 515:6611–6614
17. Ni J, Yan H, Wang A, Yang Y, Stern CL, Metz AW, Jin S, Wang L, Marks TJ, Ireland JR, Kannewurf CR (2005) MOCVD-derived highly transparent, conductive zinc- and tin- doped indium oxide thin films: precursor synthesis, metastable phase film growth and characterization, and application as anodes in polymer light-emitting diodes. J Am Chem Soc 127:5613–5624
18. Ho WH, Yen SK (2006) Preparation and characterization of indium oxide film by electrochemical deposition. Thin Solid Films 498:80–84
19. Qiao ZH, Mergel D (2005) Comparison of radio-frequency and direct-current magnetron sputtered thin In_2O_3:Sn films. Thin Solid Films 484:146–153
20. Elam JW, Martinson ABF, Pellin MJ, Hupp JT (2006) Atomic layer deposition of In_2O_3 using cyclopentadienyl indium: a new synthetic route to transparent conducting oxide films. Chem Mater 18:3571–3578
21. Jaouadi M, Gaidi M, Ezzaouia H (2013) Effect of LiBr pore-filling on morphological, optical and electrical properties of porous silicon membrane. Superlattice Microst 54:172–180
22. Huang F, Guo B, Li S, Fu J, Zhang L, Lin G, Yang Q, Cheng Q (2019) Plasma-produced ZnO nanorod arrays as an antireflective layer in c-Si solar cells. J Mater Sci. https://doi.org/10.1007/s10853-018-3099-1
23. Harraz FA, Sakka T, Ogata YH (2003) Immersion plating of nickel onto a porous silicon layer from fluoride solutions. Phys Status Solidi A 197:51–56
24. Savarimuthu E, Lalithambika KC, Moses Ezhil Raj A, Nehru LC, Ramamurthy S, Thayumanavan A, Sanjeeviraja C, Jayachandran M (2007) Synthesis and materials properties of transparent conducting In_2O_3 films prepared by sol–gel-spin coating technique. J Phys Chem Solids 68:1380–1389
25. Sariket D, Shyamal S, Hajra P, Mandal H, Bera A, Maity A, Kundu S, Bhattacharya C (2017) Temperature controlled fabrication of chemically synthesized cubic In_2O_3 crystallites for improved photoelectrochemical water oxidation. Mater Chem Phys 201:7–17
26. Prathap P, Dahiya AS, Srivastava M, Srivastava SK, Sivaiah B, Haranath D, Vandana, Srivastava R, Rauthan CMS, Singh PK (2014) Anti-reflection In_2O_3 nanocones for silicon solar cells. Sol Energy 106:102–108
27. Chen S, Manders JR, Tsang SW, So F (2012) Metal oxides for interface engineering in polymer solar cells. J Mater Chem 22: 24202–24212
28. Meyer J, Hamwi S, Kröger M, Kowalsky W, Riedl T, Kahn A (2012) Transition metal oxides for organic electronics: energetic, device physics and applications. Adv Mater 24:5408–5427
29. Arafat MM, Dinan B, Akbar SA, Haseeb A (2012) Gas sensors based on one dimensional nanostructured metal-oxides: a review. Sensors 12:7207–7258
30. Golovanov V, Maeki-Jaskari MA, Rantala TT, Korotcenkov G, Brinzari V, Cornet A, Morante J (2005) Experimental and theoretical studies of indium oxide gas sensors fabricated by spray pyrolysis. Sensors Actuators B Chem 106:563–571
31. Rahmani M, Moadhen A, Zaibi M-A, Elhouichet H, Oueslati M (2008) Photoluminescence enhancement and stabilisation of porous silicon passivated by iron. J Lumin 128:1763–1766
32. Arnoldbik WM, Habraken FHPM (2007) Swift heavy ion induced modifications of silicon (sub) oxide nitride layer structures. Nucl Instrum Methods Phys Res Sect B 256:300–304
33. Kanemitsu Y, Okamoto S (1997) Resonantly excited photoluminescence from porous silicon: effects of surface oxidation on resonant luminescence spectra. Phys Rev B 56(1696): R1696–R1699
34. Maruyama T, Ohtani S (1994) Photoluminescence of porous silicon exposed to ambient air. Appl Phys Lett 65:1346–1348
35. Kanemitsu Y, Futagi T, Matsumoto T, Mimura H (1994) Origin of the blue and red photoluminescence from oxidized porous silicon. Phys Rev B 49:14732
36. Parler CM, Ritter JA, Amiridis MD (2001) Infrared spectroscopic study of sol–gel derived mixed-metal oxides. J Non-Cryst Solids 279:119–125

37. Hamadache F, Renaux C, Duvail JL, Bertrand P (2003) Interface investigations of iron and cobalt metallized porous silicon: AES and FTIR analyses. Phys Status Solidi A 197:168–174
38. Cordoba RA, Fierro JLG, Viniegra M (1996) Study of xerogel–glass transition of CuO/SiO_2. J Solid State Chem 123:93–99
39. Parler CM (2001) Infrared spectroscopic study of sol–gel derived mixed-metal oxides. J Non-Cryst Solids 279:119–125
40. Bouzara C, Kaci S, Boukezzata A, Kezzoula F, Bozetine I, Keffous A, Trari M, Manseri A, Menari H, Azzouz R, Leitgeb M, Ouadfel MA, Talbi L, Benfadel K, Ouadah Y (2018) Study of optical properties of nanocrystalline zinc phosphide thin films. Silicon 11:331–337. https://doi.org/10.1007/s12633-018-9866-4
41. Habubi NF, Ismail RA, Mishjil KA, Hassoon KI (2018) Increasing the silicon solar cell efficiency with nanostructured SnO_2 anti-reflecting coating films. Silicon 11:543–548. https://doi.org/10.1007/s12633-017-9727-6
42. Ahmadivand A, Pala N (2015) Absorption enhancement in ultrathin structures based on crystalline-Si/Ag parabola nanocones periodic arrays with broadband antireflection property. Silicon 9:25–29. https://doi.org/10.1007/s12633-015-9341-4
43. Derbali L, Ezzaouia H (2013) Electrical properties improvement of multicrystalline silicon solar cells using a combination of porous silicon and vanadium oxide treatment. Appl Surf Sci 271:234–239
44. Zarroug A, Haddadi I, Derbali L, Ezzaouia H (2015) LiBr treated porous silicon used for efficient surface passivation of crystalline silicon solar cells. Superlattice Microst 80:181–187
45. Najar A, Elhouichet H, Lorrain N, Oueslati M (2006) Excitation mechanisms and localization sites of erbium-doped porous silicon. Appl Surf Sci 252:5808–5813
46. Laatar F, Hassen M, Smida A, Riahi R, Bel Haj Mohamed N, Ezzaouia H (2015) Effect of air-annealing on the morphological, microstructural and optical properties of CdSe NCs grown into porous anodic alumina template. Superlattice Microst 83:575–587
47. Bessais B, BenYounes O, Ezzaouia H, Mliki N, Boujmil MF, Oueslati M, Bennaceur R (2000) Morphological changes in porous silicon nanostructures: non-conventional photoluminescence shifts and correlation with optical absorption. J Lumin 90:101–109
48. Mavi HS, Rasheed BG, Shukla AK, Soni RK, Abbi SC (2003) Photoluminescence and Raman study of iron-passivated porous silicon. J Mater Sci Eng B 97:239–244
49. Rahmani M, Moadhen A, Zaibi MA, Elhouichet H, Oueslati M (2008) Photoluminescence enhancement and stabilization of porous silicon passivated by iron. J Lumin 128:1763–1766
50. Pap AE, Kordás K, Vähäkangas J, Uusimäki A, Leppävuori S, Pilon L, Szatmári S (2006) Optical properties of porous silicon. Part III: comparison of experimental and theoretical results. J Optic Mater 28:506–513
51. Riahi R, Derbali L, Ouertani B, Ezzaouia H (2017) Temperature dependence of nickel oxide effect on the optoelectronic properties of porous silicon. Appl Surf Sci 404:34–39
52. Bouznif Z, Zarroug A, Hamed ZB, Derbali L, Ezzaouia H (2018) Passivation of crystalline silicon surface treated by erbium oxides (Er_2O_3) for enhancement the photovoltaic properties. Surf Rev Lett 28:1850099
53. Salem M, Alami ZY, Bessais B, Chahboun A, Gaidi M (2015) Structural and optical properties of ZnO nanoparticles deposited on porous silicon for mc-Si passivation. J Nanopart Res 17:137